J. Plasma Physics (2000), *vol.* 64, *part* 3, *pp.* 263–273. Printed in the United Kingdom

Ion transport in glow discharges with dust

A. P. SUN, M. GENG and X. M. QIU

Southwestern Institute of Physics, PO Box 432, Chengdu 610041, PR China
(luosun@hotmail.com)

(Received 10 January 2000)

Abstract. A Monte Carlo method is used to simulate ion transport in a radiofrequency parallel-plate glow discharge with a negative-voltage pulse connected to the electrode. The dust generated during the discharge and a self-consistent electric field are taken into account. Charge exchange and elastic collisions between ions and neutral atoms and the collection and Coulomb scattering of ions on the dust particles are examined during the motion of ions in the sheath. It is found that self-consistent field, neutral gas pressure, and dust charge, dust concentration and dust size influence, to varying degrees, the energy distribution and density of ions arriving at the target, and in particular, the dust charge and concentration have significant influences. As they increase, the number of ions arriving at the target is greatly reduced. In summary, although the dust content is very low (of order 10^{-3}) in most plasma processing devices, its influence cannot be neglected, because of the large dust size and charge (in particular, the former). Therefore, in order to produce good results with ion implantation, coating, stripping, and etching, it is necessary to reduce the dust content and control the size of dust particles.

1. Introduction

Examples of plasma-generated dust particles are found in practically all plasma processes, including deposition, etching, and sputtering (Spears et al. 1986; Selwyn et al. 1989; Jellum et al. 1991; Fridman et al. 1996). These particles result from gas-phase nucleation, polymerization, or sputtering of electrode and wall surfaces. Although glow discharges contaminated by dust particles are generally not a desired operational state of these devices, they have still been the subject of many experimental studies (McCaughey and Kushner 1991a).

When dust is introduced into a plasma, it can become negatively charged because the electron and ion fluxes to the dust particle surface are unequal owing to the usually higher electron thermal speed (Mace and Hellberg 1993). The dust particles in a plasma, because of their significant negative charge, behave as an aerosol. Different dust particles in different plasmas behave similarly in many respects (Selwyn 1991).

When a negative voltage is applied to an electrode, electrons are rapidly repelled, whereas ions and dust particles basically remain stationary, and hence an ion matrix sheath is formed. The sheath field can achieve an order of magnitude of 10^3 V cm^{-1}. During the movement of ions towards the electrode, the particles remain suspended in the plasma sheath because of their larger mass and because the sheath field overcomes the gravitational force.

The particle size can vary from a few nanometres to a few millimetres (Nitter 1996), with 0.1–1.0 μm being the most common range (Winske and Jones 1994). The range of dust particle density measured in most experiments is 10^3–10^8 cm^{-3} (Winske and Jones 1994). The observed densities for relative small particles (10–100 nm) are often very high, even up to 10^9 cm^{-3}. The particles may have different shapes, but are often spherical (Nitter 1996). The dust charge q_d can reach a value of 10^3 e, where e is the elementary charge, or even 10^4 e (Tsytovich and Havnes 1993).

The use of plasmas has become indispensable in the field of material processing. However, plasmas are easily contaminated by dust particles. This kind of contamination has presented a serious problem, because it leads to a deterioration in the quality of deposited films, the yield of the fabricated device, and the effects of surface modification. On the other hand, with progress in studies on dusts, the relevant dust phenomena have begun to be considered from a new viewpoint in terms of the birth of material in plasmas. Attempts have been made to utilize dust particles nucleated in the gas phase for the preparation of supermolecules, which possess properties different from those of contentional molecules and bulk solids. A new approach in which some special ultrafine particles are injected as seeds into plasmas for growth and/or charging has been proposed in order to produce Coulomb solids and/or new materials (Watanabe 1997).

Studies on dust phenomena in plasmas, such as dust charging (Kortshagen and Mümben 1996), transport (Selwyn 1991; Barnes et al. 1992; Hwang and Keller 1996; Hwang and Kushner 1997), crystallization (Selwyn 1991; Thomas et al. 1994; Morfill and Thomas 1996; Hayashi and Tachibana 1996; Melandsø and Goree 1996; Pieper et al. 1996), dust–plasma interaction (Winske and Jones 1994; Nitter 1996), have been greatly accelerated for the reasons described above. Transport, including ion transport, dust particle transport, and electron transport, is one of the most important research topics. Monte Carlo simulations have been used to calculate the electron energy distribution (Bouchole et al. 1991; Melzer et al. 1996), the force on dust particles due to ions (McCaughey and Kushner 1989, 1991b), and particle growth and transport (Hwang and Keller 1996). In the processes such as ion implantation, ion coating, and ion stripping, a negative voltage is applied to the electrode to direct ions toward the target and increase the energy of ions arriving at the target. However, during the motion of ions within the sheath, they are scattered or collected by dust particles, so dust will affect the ion energy, density, and distribution at the target, thereby affecting the results of implantation, coating, and stripping. In this paper, we focus attention on ion transport in the presence of dust particles, and use a Monte Carlo method to simulate ion transport in a radiofrequency parallel-plate glow discharge with a negative-voltage pulse connected to the electrode. For simplicity in the mathematical treatment, in the simulation, we assume the dust density to be uniform. In addition, we consider the dust density, charge, and size, which are variables, as parameters. We then choose individual typical values of these parameters, and examine their influence on the energy distribution and density of ions arriving at the target.

The remainder of the paper is organized as follows. In Sec. 2, a basic model of simulation is presented. The simulation results and analyses are given in Sec. 3. Section 4 is devoted to a discussion and conclusions.

2. Basic model

When a negative voltage is applied to a planar electrode, the electrons near the electrode surface are driven away on a time scale of the inverse electron plasma frequency ω_{pe}^{-1}:

$$t = \frac{\lambda_{D0}}{\langle v \rangle} = \left(\frac{\varepsilon_0 kT_e}{n_0 e^2}\right)^{1/2} \Big/ \left(\frac{kT_e}{m_e}\right)^{1/2} = \left(\frac{\varepsilon_0 m_e}{n_0 e^2}\right)^{1/2} = \omega_{pe}^{-1}, \tag{1}$$

where λ_{D0} is the electron Debye length, $\langle v \rangle$ the electron thermal velocity, ε_0 the vacuum permittivity, k Boltzmann's constant, T_e the electron temperature, n_0 the plasma density, and m_e the electron mass. Subsequently, ions inside the sheath are accelerated towards the target. Ion trajectories are computed by Monte Carlo techniques. Initial velocities are randomly chosen from a Maxwellian distribution with the neutral-gas temperature, and the ions starting at the sheath edge are directed towards the target. The ions are accelerated by the total electric field $\mathbf{E}_{\text{tot}} = \mathbf{E}_{\text{appl}} + \mathbf{E}_{\text{self}}$, where $\mathbf{E}_{\text{appl}}$ is produced by the applied negative-voltage and $\mathbf{E}_{\text{self}}$ is the self-consistent electric field. During the motion of ions, they may collide with neutral atoms and dust particles, and then be accelerated again. This process continues until the ions strike the target. The charge exchange and elastic collision between ions and neutral atoms and the collection and Coulomb scattering of ions by dust particles are included in the computation.

We take the x axis to be directed to the electrode and the origin to be at the sheath edge. θ is the angle between the ion direction of motion and the x axis. We assume that the gas discharge is uniform and stable. At the beginning of the simulation, $\mathbf{E}_{\text{self}} = 0$, and so

$$E_{\text{tot}} = \frac{2U_0 x}{d^2}, \tag{2}$$

where U_0 is the magnitude of the applied negative voltage and d the sheath width.

The ions are tracked from the plasma sheath edge ($x = 0$) until they are collected by dust or arrive at the electrode. The ion velocity $v_i(x)$ and the number of ions $N_i(x)$ at each position are recorded, and the average ion velocity at each position $\overline{v_i(x)}$ is calculated. We can compute the new $\mathbf{E}_{\text{tot}}$ according to the following two formulae:

$$n_i(x+dx)\,\overline{v_i(x+dx)} - n_i(x)\,\overline{v_i(x)} = -n_i(x)\,\overline{v_i(x)}\left[1 - \frac{N_i(x+dx)}{N_i(x)}\right], \tag{3}$$

where n_i is the ion density, and

$$\mathbf{E}_{\text{tot}}(x+dx) - \mathbf{E}_{\text{tot}}(x) = \int_x^{x+dx} [q_i\, n_i(x') + q_d\, n_d]\, dx', \tag{4}$$

where q_i is the ion charge, q_d the dust charge, and n_d the dust density, which is assumed to be uniform. We then repeat the above steps until $\mathbf{E}_{\text{tot}}$ converges.

From now on, we continue to examine the motion of ions under the converged $\mathbf{E}_{\text{tot}}$ in the sheath. In a distance Δx (taken to be $\frac{1}{10}\lambda$, where λ is the ion mean free

https://doi.org/10.1017/S0022377800008552 Published online by Cambridge University Press

path), the probabilities of charge exchange and elastic collision between an ion and a neutral atom are respectively

$$P_{\rm ex} = \frac{n_n \sigma_{\rm ex}(\varepsilon_c)\,\Delta x}{|\cos\theta|}, \tag{5}$$

$$P_{\rm elast} = \frac{n_n \sigma_{\rm elast}(\varepsilon_c)\,\Delta x}{|\cos\theta|}. \tag{6}$$

Analogously, the probabilities of Coulomb scattering and collection of an ion by a dust particle are respectively

$$P_{\rm coul} = \frac{n_d \sigma_{\rm Coul}(\varepsilon_c)\,\Delta x}{|\cos\theta|}, \tag{7}$$

$$P_{\rm coll} = \frac{n_d \sigma_{\rm coll}(\varepsilon_c)\,\Delta x}{|\cos\theta|}, \tag{8}$$

where n_n is the neutral-gas density, ε_c the ion energy at position $x+\frac{1}{2}\Delta x$, n_d the dust particle density, and $\sigma_{\rm ex}$, $\sigma_{\rm elast}$, $\sigma_{\rm Coul}$, and $\sigma_{\rm coll}$ the cross-sections for charge exchange, elastic collision, Coulomb scattering and collection respectively.

When a charge-exchange collision between an ion and a neutral atom occurs, the energy of the newly produced ion is chosen randomly from a Maxwellian distribution with the neutral-gas temperature (Wang et al. 1993). The scattering angle χ and the azimuthal angle ϕ of the newly produced ion with respect to the trajectory of the original ion are isotropic. That is,

$$x = r_1 \pi, \tag{9}$$

$$\phi = r_2 2\pi, \tag{10}$$

where r_1 and r_2 are uniform random numbers between 0 and 1.

For elastic collisions between ions and neutral atoms, we use the hard-sphere model with equal masses; then

$$\varepsilon_1 = \varepsilon \cos^2\chi \tag{1}$$

where ε and ε_1 are the energy of the incident and scattered ions respectively. The scattering angle χ is obtained from

$$\cos\chi = \sqrt{1-r_3}, \tag{12}$$

and the azimuthal angle ϕ is uniform,

$$\phi = r_4 2\pi, \tag{13}$$

where r_3 and r_4 are uniform random numbers between 0 and 1.

We take the neutral gas to be argon (Ar) and employ the following formulae to calculate the charge-exchange cross-section $\sigma_{\rm ex}$ and elastic-collision cross-section $\sigma_{\rm elast}$ between Ar^+ and Ar:

$$\sigma_{\rm ex}(\varepsilon) = (59.21 - 4.61\ln\varepsilon)\times 10^{-16}\ {\rm cm}^2, \tag{14}$$

$$\sigma_{\rm elast}(\varepsilon) = (118.90 - 9.85\ln\varepsilon)\times 10^{-16}\ {\rm cm}^2; \tag{15}$$

https://doi.org/10.1017/S0022377800008552 Published online by Cambridge University Press

for $\varepsilon < 0.1$ eV, we can take $\sigma_{ex} = 69.82 \times 10^{-16}$ cm^2 and $\sigma_{elast} = 157.00 \times 10^{-16}$ cm^2.

For Coulomb scattering of ions by dust particles, because of the great disparity in mass between the two, the energy of the scattered ion does not change. The scattering cross-section σ_{Coul} is given by (Nitter 1996)

$$\sigma_{Coul} = 2\pi b_0^2 \ln \Lambda, \tag{16}$$

$$\Lambda = \frac{\lambda_D^2 + b_0^2}{b_{coll}^2 + b_0^2}. \tag{17}$$

where $\ln \Lambda$ is the Coulomb logarithm; b_0 is the impact parameter corresponding to a 90° deflection, and can be represented as

$$b_0 = \frac{q_i q_d}{4\pi\varepsilon_0 m_i v_i^2}, \tag{18}$$

with m_i being the ion mass and v_i the ion velocity; b_{coll} is the impact parameter for an ion grazing the dust particle,

$$b_{coll} = a\left(1 - \frac{2b_0}{a}\right)^{1/2}, \tag{19}$$

with a being the dust radius; λ_D is the local electron Debye length,

$$\lambda_D = \left(\frac{\varepsilon_0 kT_e}{n_e e^2}\right)^{1/2}, \tag{20}$$

with n_e being the local electron density. In the presence of the local potential V due to the $\mathbf{E}_{tot}$, the local electron density obeys the following Boltzmann relation:

$$n_e = n_0 \exp\left(\frac{eV}{kT_e}\right). \tag{21}$$

We denote the potential around the dust particle by V_d. It is easy to show that (Nitter 1996)

$$V_d = \frac{q_d}{4\pi\varepsilon_0 a}. \tag{22}$$

The scattering angle of an ion by a dust particle is

$$\chi = \frac{2q_i q_d}{4\pi\varepsilon_0 m_i v_i^2 b}, \tag{23}$$

where b is the impact parameter; the azimuthal angle ϕ is uniform,

$$\phi = r_5 2\pi, \tag{24}$$

where r_5 is a uniform random number between 0 and 1. After the scattering of an ion by a neutral atom or a dust particle, the angle θ' between the ion direction of motion and the x axis is calculated from the formula

$$\cos\theta' = \cos\theta\cos\chi + \sin\theta\sin\chi\cos\phi. \tag{25}$$

https://doi.org/10.1017/S0022377800008552 Published online by Cambridge University Press

The cross-section for the collection of ions by dust particles is

$$\sigma_{\mathrm{coll}} = \pi b_{\mathrm{coll}}^2. \tag{26}$$

If an ion does not collide with any neutral atoms or dust particles within a distance Δx then its new position x_1 and energy ε_1 are respectively

$$x_1 = x + \Delta x \tag{27}$$

$$\varepsilon_1 = \varepsilon + q_i E_{\mathrm{tot}}(x)\,\Delta x \tag{28}$$

3. Simulation results and analysis

A radiofrequency parallel-plate glow discharge with working gas of argon and the following related parameters are taken for simulation of ion transport. The target is immersed in an argon plasma with a density $n_0 = 5 \times 10^9$ cm^{-3}. The negative-voltage pulses $U_0 = 100$ V and the initial ion matrix sheath width $s_0 = (2\varepsilon_0 U_0/en_0)^{1/2}$. The neutral-gas temperature $T_n = 0.025$ eV, the electron temperature $T_e = 2$ eV, the ion temperature $T_i = 0.04$ eV, and the working-gas pressure $P = 1.33$ Pa. The sheath width is assumed to be 1 cm.

In the present simulation, there is a self-consistent field $\mathbf{E}_{\mathrm{self}}$ besides the applied field $\mathbf{E}_{\mathrm{appl}}$. The ions are accelerated by the sum $\mathbf{E}_{\mathrm{tot}}$ of the two fields. Therefore we first have to compute the converging total field $\mathbf{E}_{\mathrm{tot}}$. Then, under the action of the total field, we simulate the motion of a large number of ions and calculate the energy distribution of ions arriving at the target and the ion density near the target. Figure 1 shows the electric field convergence processes. We can see that the computation only needs to be repeated four times to converge $\mathbf{E}_{\mathrm{tot}}$.

Figure 2 shows the effect of dust on the energy distributions of the ions at the target. It can be seen that in the presence of dust, the proportion of low-energy ions increases and that of high-energy ions decreases. The reason is that some of the accelerated ions are collected by the dust particles before they arrive at the target. In addition, the nearer the target, the weaker is the total field strength with dust than without dust (see Fig. 1). Figure 3 depicts the influence of dust density on the ion energy distribution. It is thus clear that when the dust density is higher, the energy distribution shifts to the low-energy region, because the probability of ions collected by the dust is proportional to dust particle density (see (8)). Meanwhile, the probability of Coulomb scattering of ions by the dust particles is also proportional to the dust particle density (see (7)). Although during Coulomb scattering, the energy of the scattered ion does not change, the direction of motion does, and hence the times of ion–neutral and/or ion–dust interaction in the sheath will increase. The effect of dust size on the ion energy distribution is plotted in Fig. 4. We can see that when the dust size is larger, the energy distribution shifts to the low-energy region again. The reasons for this effect are as follows: first, the probability of ions collected by the dust is almost proportional to the square of the dust size (see (8), (26), and (19)); secondly, for 0.5 cm $< x \leqslant 1$ cm, the converged total field is weaker for larger dust size than for smaller (compare Figs 1(b) and (c)). Figure 5 shows the influence of dust charge on the ion energy distribution at the target. It is found that as the dust charge increases, the energy distribution shifts to the low-

https://doi.org/10.1017/S0022377800008552 Published online by Cambridge University Press

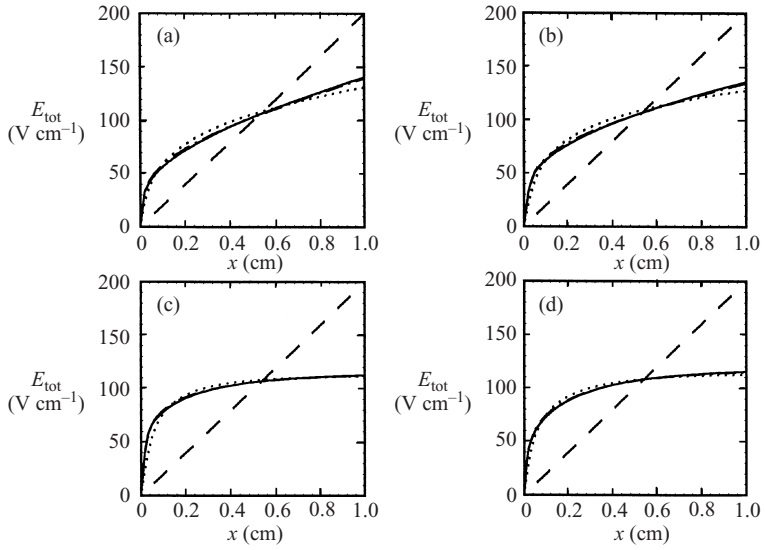

Figure 1. The convergence process for E_{tot}: ———, initial E_{tot} (Conrad 1987); ....., second simulation; – – – –, third simulation; ——, fourth simulation (on the scale of the figures, the third and fourth simulations are virtually indistinguishable). (a) Without dust; (b) $n_d = 5 \times 10^6$ cm^{-3}, $a = 1.0$ μm, $q_d = 10^3$ e; (c) $n_d = 5 \times 10^6$ cm^{-3}, $a = 0.1$ μm, $q_d = 10^3$ e; (d) $n_d = 5 \times 10^6$ cm^{-3}, $a = 1.0$ μm, $q_d = 10^2$ e.

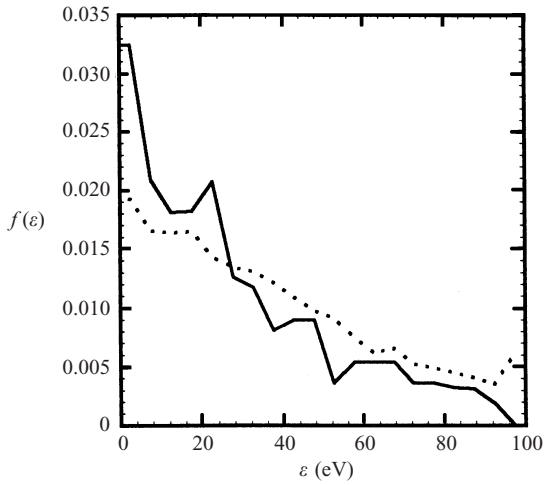

Figure 2. The effect of dust on the energy distribution of dust particles at the target: ....., without dust; ——, with dust.

energy region again. The reason for this is that when the dust charge q_d increases, both the cross-section for Coulomb scattering of ions by dust particles and the scattering angle become large (see (16), (18), and (23), leading to the increases in the times of ion–neutral and/or ion–dust interaction in the sheath.

Figure 6 depicts the change of ion density at the target with dust concentration (for different dust sizes), i.e. the ratio of dust particle density to

https://doi.org/10.1017/S0022377800008552 Published online by Cambridge University Press

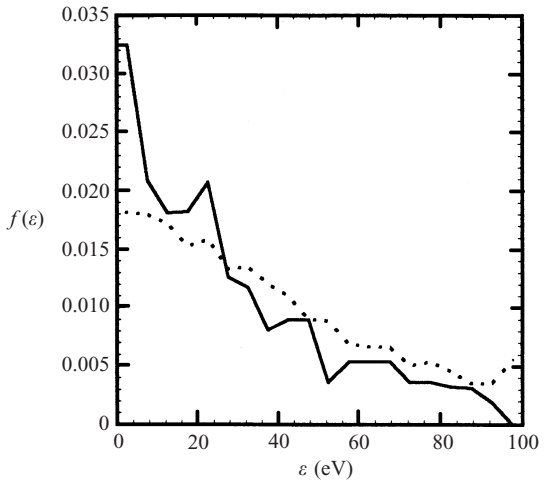

Figure 3. The influence of dust density on the energy distribution at the target: ....., $n_d = 1 \times 10^6$ cm^{-3}, $a = 1.0$ μm, $q_d = 10^3$ e; ——, $n_d = 1 \times 10^7$ cm^{-3}, $a = 1.0$ μm, $q_d = 10^3$ e.

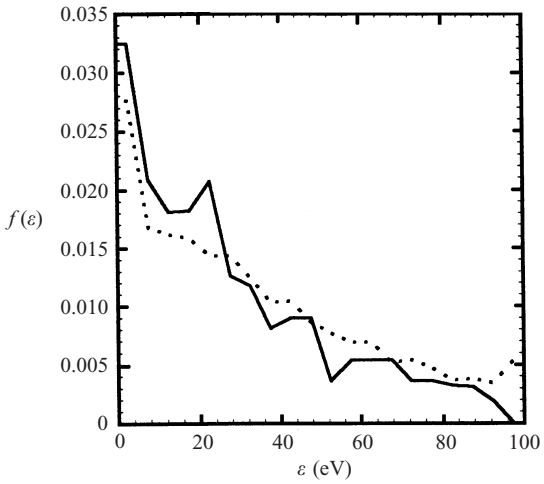

Figure 4. The effect of dust size on the energy distribution at the target: ....., $n_d = 1 \times 10^7$ cm^{-3}, $a = 0.1$ μm, $q_d = 10^3$ e; ——, $n_d = 1 \times 10^7$ cm^{-3}, $a = 1.0$ μm, $q_d = 10^3$ e.

initial ion density, n_d/n_{i0}, where $n_{i0} = n_i(x = 0)$. We can see that the ion density at the target drops rapidly with increasing n_d/n_{i0}. The reason for this is that the probability for ions to be collected by the dust is proportional to the dust particle density, and a uniform dust particle density in the sheath is assumed in this paper. We can also see that the ion density falls much more rapidly with larger dust size than with smaller. The reason for this is that the probability of collection of ions by the dust is almost proportional to the square of the dust size. The change in ion density at the target with dust size for different dust densities is shown in Fig. 7. We find that the ion density falls much more rapidly

https://doi.org/10.1017/S0022377800008552 Published online by Cambridge University Press

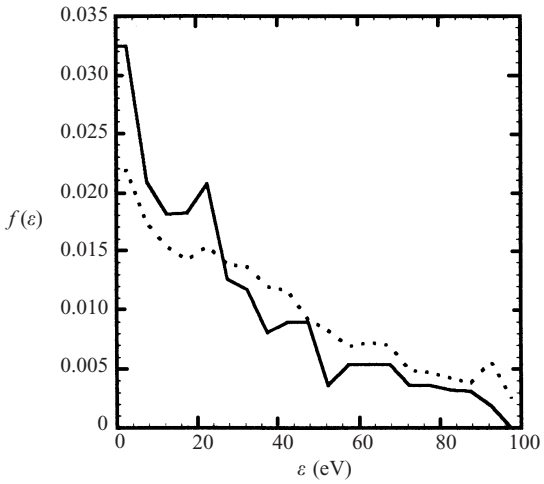

Figure 5. The influence of dust charge on the energy distribution at the target: ....., $n_a = 1 \times 10^7$ cm^{-3}, $a = 1.0$ μm, $q_a = 10^2$ e; ——, $n_a = 1 \times 10^7$ cm^{-3}, $a = 1.0$ μm, $q_a = 10^3$ e.

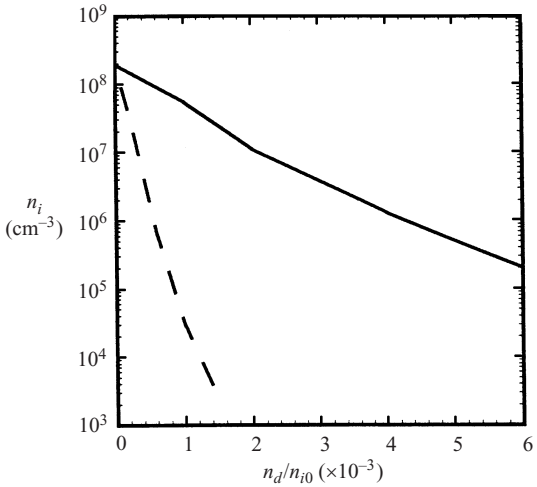

Figure 6. Ion density at the target versus dust density for different dust sizes: ——, $a = 0.3$ μm, $q_a = 10^3$ e; ———, $a = 1.0$ μm, $q_a = 10^3$ e.

in the case of higher dust density. We have calculated the change in ion density at the target with dust charge. The result indicates that the change is less considerable. The reason for this is that the dust charge mainly influences the Coulomb scattering of ions by dust particles (see (16), (18), and (23)), and only exerts a slight influence on the collection of ions by dust particles (see (18) and (19)). In other words, the increase in dust charge mainly leads to increases in the times of ion–neutral and/or ion–dust interaction in the sheath before ions arrive at the target.

https://doi.org/10.1017/S0022377800008552 Published online by Cambridge University Press

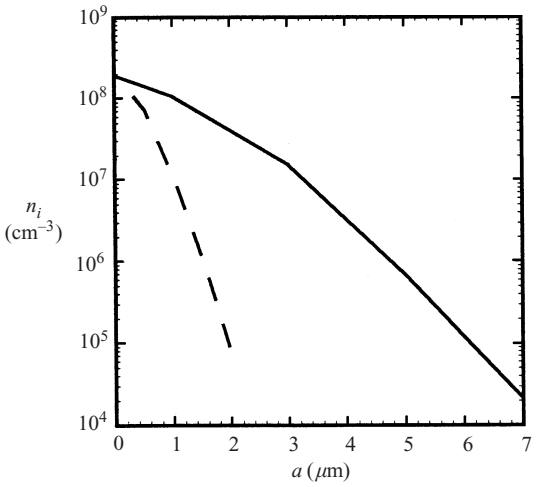

Figure 7. Ion density at the target versus dust size for different dust densities: ——, $n_d = 1 \times 10^6$ cm^{-3}, $q_d = 10^3\, e$; ———, $n_d = 1 \times 10^7$ cm^{-3}, $q_d = 10^3\, e$.

4. Discussion and conclusions

We have simulated ion transport in glow discharges with dust. We have found that self-consistent electric field, neutral gas pressure, dust charge, dust concentration, and dust size influence, to varying degrees, the energy distribution and density of ions (especially, the density) arriving at the target, and, in particular, the dust concentration and size have significant influences. To be specific, as the dust concentration or dust size increases, the number of ions arriving at the target falls greatly.

The conclusions drawn from the simulation results are in complete agreement with the qualitative analyses that we have made according to the property of a self-consistent field and the laws of ion–neutral and ion–dust interaction. In conclusion, although the dust content is very low (of order 10^{-3}) in most plasma processing devices, its influence is important because of large size and charge (in particular, the former). Therefore, in order to produce good results with ion-implantation, coating, stripping, and etching, it is necessary to reduce the dust content and control the size of dust particles.

In the case of a concentration of 6×10^{-3} or a size of 2 μm, the ion density at the target is reduced by a factor of 10^3 or 3×10^3 (see Figs 6 and 7). This is an approximation, because in the simulation, we have assumed the dust density to be uniform (in practice, it is locally uniform in most devices). In forthcoming work, we shall improve our code to consider dust with non-uniform dust density and size distributions. Also, we shall take secondary electron emission into account.

Acknowledgements

We should like to acknowledge helpful discussions with Professor Z. K. Shang and to express our appreciation to Professor W. B. Xu for his help in computation.

References

Barnes, M. S., Keller, J. H., Forster, J. C. et al. 1992 *Phys. Rev. Lett.* **68**, 313.
Bouchoule, A., Plain, A., Boufendi, L. et al. 1991 *J. Appl. Phys.* **70**, 1001.
Conrad, J. R. 1987 *J. Appl. Phys.* **62**, 777.
Fridman, A. A., Boufendi, L., Hbid, T. et al. 1996 *J. Appl. Phys.* **79**, 1303.
Hayashi, Y. and Tachibana, K. 1996 *J. Vac. Sci. Technol.* **A14**, 506.
Hwang, H. H. and Keller, M. T. 1996 In: *Conference Record–Abstracts IEEE International Conference on Plasma Science, Boston, 3–5 June 1996*, p. 176. IEEE, New York.
Hwang, H. H. and Kushner, M. J. 1997 *J. Appl. Phys.* **82**, 2106.
Jellum, G. M., Daugherty, J. E. and Graves, D. B. 1991 *J. Appl. Phys.* **69**, 6923.
Kortshagen, U. and Mümben, G. 1996 *Phys. Lett.* **217A**, 126.
McCaughey, M. J. and Kushner, M. J. 1989 *Appl. Phys. Lett.* **55**, 951.
McCaughey, M. J. and Kushner, M. J. 1991a *J. Appl. Phys.* **69**, 1952.
McCaughey, M. J. and Kushner, M. J. 1991b *J. Appl. Phys.* **69**, 6952.
Mace, R. L. and Hellberg, M. A. 1993 *Planet. Space Sci.* **41**, 235.
Melandsø, F. and Goree, J. 1996 *J. Vac. Sci. Technol.* **A14**, 511.
Melzer, A., Schweigert, V. A., Schweigert, I. V. et al. 1996 *Phys. Rev.* **E54**, R46.
Morfill, G. E. and Thomas, H. 1996 *J. Vac. Sci. Technol.* **A14**, 490.
Nitter, T. 1996 *Plasma Sources Sci. Technol.* **5**, 93.
Pieper, J. B., Goree, J. and Quimn, R. A. 1996 *J. Vac. Sci. Technol.* **A14**, 519.
Selwyn, G. S. 1991 *J. Vac. Sci. Technol.* **B9**, 3487.
Selwyn, G. S., Singh, J. and Bennett, R. S. 1989 *J. Vac. Sci. Technol.* **A7**, 2758.
Spears, K. G., Robinson, T. M. and Roth, R. M. 1986 *IEEE Trans. Plasma Sci.* **14**, 179.
Thomas, H., Morfill, G. E., Demmel, V. et al. 1994 *Phys. Rev. Lett.* **73**, 652.
Tsytovich, V. N. and Havnes, O. 1993 *Comments Plasma Phys. Contr. Fusion* **15**, 267.
Wang, D. Z., Ma, T. C. and Gong, Y. 1993 *J. Appl. Phys.* **79**, 4171.
Watanabe, Y. 1997 *Plasma Phys. Contr. Fusion* **39**, A59.
Winske, D. and Jones, M. E. 1994 *IEEE Trans. Plasma Sci.* **22**, 454.